Crystallization Pathway of Size-Controlled SnO 2 Nanoparticles Synthesized via a Nonaqueous Sol–Gel Route

Alex Lemarchand, Fabien Remondiere, Jenny Jouin, Philippe Thomas, Olivier Masson

Crystallization pathway of size-controlled SnO2 nanoparticles synthesized via a nonaqueous sol-gel route

Journal:	*Inorganic Chemistry*
Manuscript ID	ic-2019-03000p
Manuscript Type:	Article
Date Submitted by the Author:	11-Oct-2019
Complete List of Authors:	Lemarchand, Alex; IRCER REMONDIERE, Fabien; Universite de Limoges, Chemistry Jouin, Jenny; Universite de Limoges, Laboratoire SPCTS Thomas, Philippe; Science des Procedes Ceramiques et de Traitements de Surface, Université de Limoges Masson, Olivier; Universite de Limoges, Chemistry

Crystallization pathway of size-controlled SnO_2 nanoparticles synthesized *via* a nonaqueous sol-gel route

*Alex Lemarchand, Fabien Rémondière, Jenny Jouin, Philippe Thomas and Olivier Masson**

Institute of Research for Ceramics, UMR 7315 CNRS - Université de Limoges, Centre Européen de la Céramique – 12, rue Atlantis 87068 Limoges

Abstract. This paper deals with the crystallization pathway of tin dioxide ultra-small nanoparticles synthesized *via* a nonaqueous sol-gel route based on the etherolysis of tin tetrachloride ($SnCl_4$) precursor. Two different ethers were used as oxygen donors: diisopropyl ether ($^iPr_2O$) and dibenzyl ether (Bn_2O). The solvothermal treatments of $SnCl_4$ in $^iPr_2O$ at different temperatures and reaction times, revealed in the early stages of the reaction the formation of an organic polymeric phase in which crystalline nanoparticles are embedded. In the case of the $SnCl_4$-Bn_2O system, the formation of a brownish polymer containing crystalline oxidic nanoparticles and the production of water were evidenced. With both ethers, an unexpected intermediate disordered nano-crystalline phase is formed, which progressively transforms into rutile-type SnO_2 nanoparticles. The formation of the polymeric phase, which is suspected to act as a trap for the nanoparticles, freezes the intermediate phase, limits the particle growth and delays the restructuration into the rutile-type structure. The

degradation of the polymer phase in the case of $^{i}Pr_2O$ and/or the water action in the case of Bn_2O are finally able to destabilize the nanoparticle-polymer assembly and to induce the restructuration of the nanoparticles.

Keywords. Nonaqueous sol-gel synthesis; Tin dioxide nanoparticles; Etherolysis; Crystallization pathway; XRD; TEM

Introduction

Tin (IV) dioxide with rutile-type structure (i.e. *cassiterite* mineral) [1] is a well-known semiconductor with a band gap of 3.6 eV at 300 K widely used as solid-state gas sensor material [2][3], oxidation catalyst [4] and transparent conductor [5]. For all these applications, a high surface area is of great importance, which in turn emphasizes the interest of producing nano-sized particles. Various synthesis methods are found in literature as for example flame pyrolysis [6], thermal evaporation [7], laser-ablation techniques [8] and the common solution chemistry methods[1]. Among the latter, sol-gel aqueous [9][10][11][12][13][14] and nonaqueous routes [15][16][17] are particularly powerful for obtaining particles of very small and controlled size. The nonaqueous method offers the advantage of producing well-crystallized nanoparticles at moderate temperature without the need of any additional post-thermal treatment [18][19][20]. Particularly interesting are the solvent-controlled syntheses in which the oxygen donor solvent also controls the particle size [18]. Among them, the so-called "benzyl alcohol route", in which benzyl alcohol is used as solvent, is one of the most versatile. This route has been applied in the case of tin oxide using both tin (IV) chloride and tin (IV) *tert*-butoxide [16][17] and allowed obtaining nanoparticles of 3.5 nm and 2.2 nm respectively. However, the use of such protic solvent can lead to a water release in the reaction medium (through solvent condensation and hydroxylation reactions), which is detrimental

for the control of the particle growth. As an alternative, the use of an aprotic oxygen donor was developed by Mutin and Vioux [19][20]. The chemical pathway involved in the formation of the nanoparticles is then simplified and the control over the final product is easier to achieve. This method was recently applied to the synthesis of SnO_2 nanoparticles [15] and is based on the reaction of $SnCl_4$ with a stoichiometric amount of diisopropyl ether. Organo-soluble and reactive SnO_2 nanoparticles exhibiting an average diameter of 4 nm with a narrow size distribution were obtained with an excellent yield. The proposed synthesis mechanism is a two-step process that consists in: (i) the etherolysis of the tin chloride precursor leading to the formation of tin isopropoxide groups and (ii) the condensation between the isopropoxide and the chloride leading to the formation of the oxidic network jointly to the release of isopropyl chloride. The corresponding chemical reactions (for one ligand only) are given below:

$$Sn - Cl + {}^{i}Pr_2O \rightarrow Sn - O{}^{i}Pr + {}^{i}PrCl \quad (1)$$

$$Sn - O - {}^{i}Pr + Sn - Cl \rightarrow Sn - O - Sn + {}^{i}PrCl \quad (2)$$

The effective control of the nanoparticle size requires the understanding of the nanoparticle formation mechanism, which is most of the time not fully understood since the classical nucleation-growth theory based on the LaMer model is not pertinent in numerous cases. Recent studies emphasize alternative pathways [21][22][23][24][25] (not simply based on the attachment of ions, atoms or molecules to form an individual cluster) such as oriented attachment, [26][27][28][29][30] mesocrystal formation [31][32] or formation of intermediate metal-organic phase. For example, Ba *et al.* [33] have recently shown that the solvothermal synthesis of indium-tin oxide (ITO) nanoparticles in benzyl alcohol was a two-stage process involving the formation of an undetermined intermediate phase. This latter, characterized by small particles connected in an

organic matrix, transforms with time into the final ITO nanoparticles during the solvothermal treatment.

In this paper, we present a study of the early stages of crystallization of SnO_2 nanoparticles obtained *via* a modified nonaqueous sol-gel synthesis inspired by the work of Aboulaich *et al.*[15]. In this context, two ethers were used. Firstly, $^{i}Pr_2O$, which already showed a great ability to produce crystalline SnO_2 nanoparticles of small size, is reinvestigated to evidence a possible unusual crystallization sequence. Secondly, Bn_2O, which is susceptible to induce spatial hindrance because of its aromatic ring and thus to induce a control on the particle size, is newly tested here. Moreover, since aromatic solvents are susceptible to polymerize and to release water, the non-hydrolytic feature of the reaction was questioned and investigated.

Experimental section

Chemicals. Tin (IV) tetrachloride ($SnCl_4$, 98%) was purchased from Strem Chemicals. Diisopropyl ether ($^{i}Pr_2O$, 99%) and dibenzyl ether (Bn_2O, 99%) were purchased from Sigma Aldrich. Other solvents used for the synthesis and the flocculation of the nanoparticles and the TEM grid preparation are respectively dichloromethane (99+%, Alfa Aesar), chloroform (99.8%, Alfa Aesar), acetone (99+%, Alfa Aesar), n-heptane (99%, Fisher Scientific), 1-butanol (99%, Alfa Aesar). All the solvents were utilized without any further purification. The anhydrous feature of the ethers was confirmed by Karl-Fisher analysis.

Synthesis of SnO_2 nanoparticles. All the manipulations were carried out in a glovebox under dry air atmosphere. The Sn^{4+} concentration was set to 0.5 $mol.L^{-1}$. This relatively high concentration was set to minimize the economic and ecological impacts of the process.

Syntheses with diisopropyl ether. The typical synthesis of the tin oxide nanoparticles was performed by adding $SnCl_4$ (5 mmol), $^{i}Pr_2O$ (15 mmol, [ether]/[Sn^{4+}]=3.0) in CH_2Cl_2, to obtain a

Sn^{4+} concentration of 0.5 mol.L^{-1}. The mixture was then transferred in a Teflon cup of 25 mL inner volume, placed in a steel autoclave, and heated at the targeted temperature under autogenous pressure. To study the influence of the reaction temperature and reaction time, the heat treatment was performed in a range of 95°C-140°C for at least 12 h and up to 140 h. All the synthesis parameters are summarized in Table 1.

Syntheses with dibenzyl ether. In this case, the synthesis of the tin oxide nanoparticles was performed by adding $SnCl_4$ (7.5 mmol) in Bn_2O (72.75 mmol, [ether]/[Sn^{4+}]=9.7) in order to obtain a total volume of 15 mL. Preliminary experiments showed that the use of an ether to tin molar ratio of 3.0 did not lead to the formation of any inorganic solid product. It was thus increased to a value of 9.7 to ensure the formation of a powder. The reactive mixture was transferred in a sealed glass tube and heated by a conventional oil bath. To study the influence of the reaction temperature and reaction time, the heat treatment was performed in a range of 95°C-140°C for at least 30 min and up to 60 h. All the synthesis parameters are summarized in Table 1.

Washing procedure, supernatant characterization and powder recuperation. The brownish suspensions obtained in the case of $^{i}Pr_2O$ were washed and centrifuged (10 minutes, 10,000 rpm) with first a 20 mL volume mixture of heptane and acetone and finally twice with 20 mL of acetone to eliminate the majority of the organic residues. The dark brown polymer obtained in the case of Bn_2O was first dissolved in several portions of chloroform under a time-consuming shaking procedure (≈ 2-4 hours). This operation was repeated until most of the polymer was dissolved and removed. The unsolubilized part of the sample was finally washed and centrifuged (10 minutes, 10,000 rpm) twice in 20 mL of chloroform, once with a 20 mL volume mixture of heptane and acetone and finally twice with 20 mL of acetone to remove as much as possible of the remaining polymer. In both cases, the as-obtained precipitate was finally collected with 15 mL of

dichloromethane and air dried overnight at room temperature. The final product was softly ground to powder for the chemical characterizations and kept a light-cream colour with a slight brownish tint. The characteristics of the synthesis products are summarized in Table 1. During the washing step, the first supernatant was isolated for each sample to highlight the potential presence of water during the synthesis. For that purpose, a test based on the colour change of anhydrous copper sulphate was performed. To this end, one drop of the suspension composed of the synthesis liquid and of the antisolvent mixture was deposited onto the anhydrous copper sulphate powder. The solvent used during the washing step were tested beforehand to ensure they were water-free.

Table 1. Experimental parameters for the synthesis of SnO_2 nanoparticles and corresponding reaction products.

Sample Label	$[Sn^{4+}]$ (mol.L^{-1})	Oxygen donor	$[ether]/[Sn^{4+}]$	Solvothermal treatment		Products
				Temperature (°C)	Reaction time (h)	
Pr-95°C-12h	0.5	$^{i}Pr_2O$	3.0	95	12	Powder, liquid supernatant
Pr-95°C-24h					24	
Pr-95°C-60h					60	
Pr-95°C-100h					100	
Pr-95°C-140h					140	
Pr-110°C-60h				110	60	
Pr-110°C-100h					100	
Pr-110°C-140h					140	
Pr-125°C-60h				125	60	
Pr-125°C-100h					100	
Pr-140°C-60h				140	60	

Bn-95°C-60h				95	60	
Bn-110°C-4h					4	Polymer,
Bn-110°C-12h				110	12	powder,
Bn-110°C-24h		Bn_2O	9.7		24	aqueous phase
Bn-110°C-60h					60	
Bn-125°C-2h				125	2	
Bn-140°C-0.5h				140	0.5	

Sample characterization. The phase identification and the structural and microstructural characterizations of the samples were performed by X-ray powder Diffraction (XRD). Data were collected with the $CuK\alpha_1$ radiation (1.5406 Å) from 10° to 110° (2θ) with a step size of 0.020° (2θ) and an equivalent counting time per step of 1567s using a Bragg-Brentano (θ-2θ) BRUKER D8 Advance diffractometer equipped with a rapid LYNXEYE detector. The diffraction patterns were treated using the Rietveld method [34][35] implemented in the Fullprof software [36][37] and by peak by peak decomposition using the Peakoc software [38]. Particle size and micro-strains were estimated using both the Pseudo-Voigt line profile function in its Thompson-Cox-Hastings formulation [39][40] (Fullprof) and the Voigt function [41] (Peakoc). The characterizations were supplemented by High-Resolution Transmission Electron Microscopy (HRTEM) and Selected Area Electron Diffraction (SAED) using a JEOL 2100f. The samples were prepared by evaporating a drop of a diluted nanoparticle suspension onto an ultrathin carbon-A holey 400 mesh copper grid. This suspension was prepared by the dilution of one drop of the final suspension obtained at the end of the washing step in 10 mL of n-butanol. The average particle size was determined from the micrographs by the analysis of a set of 30 particles for each sample. For two samples, the 1D

electron powder diffraction diagrams were obtained by integrating sectors of the SAED images using the FIT2D software [42].

Results and discussion

Syntheses with diisopropyl ether. The copper sulphate test conducted on the first synthesis supernatant was negative for all the samples synthesized using $^{i}Pr_2O$ indicating that the formation mechanism of the SnO_2 nanoparticles by this procedure is non-hydrolytic. The XRD patterns of the samples prepared with $^{i}Pr_2O$ at 95°C, 110°C, 125°C and 140°C between 12 h and 140 h are plotted in Figure 1. For the syntheses at 125°C and 140°C, the diagrams are typical of a single rutile-type phase. This is confirmed by the good quality Rietveld refinements obtained for these samples (Figure 2). The refined microstructural parameters correspond to a negligible amount of microstrains and average particle diameters of about 3.7 nm and 3.3 nm for 140°C (60h) and 125°C (100h) respectively. For a synthesis time reduced to 60 h at 125°C, the average particles diameter decreases to about 2.7 nm. For lower temperatures (110°C and 95°C), the evolution of the XRD patterns does not suggest a simple particle size decrease, but instead some important structural changes. At 110°C, when the synthesis reaction time is reduced from 140 h to 60 h, the 110 peak undergoes an huge asymmetric enlargement and a shift of its maximum position from $2\theta = 26.5°$ to $2\theta = 27.5°$ whereas the 101 peak remains almost unchanged in terms of width and position. In addition, two peaks appear at $2\theta = 18.0°$ and 23.5°. The rest of the diagram mainly undergoes a progressive enlargement, with the exception of the 301 peak which disappears progressively. At 60h, the XRD diagram has clearly very broad lines apart from the narrow 101 peak. A similar feature was already observed by Aboulaich *et al.* for samples synthesized following an equivalent synthesis method but was not considered further [15]. At 95°C, for reaction times decreasing from

140 h to 60 h, the diagrams keep evolving similarly to finally exhibit only a narrow 101 peak and two small bumps at 2θ = 18.0° and 23.5°. When the reaction time is further reduced to less than 24 h, these features are hardly noticeable but present.

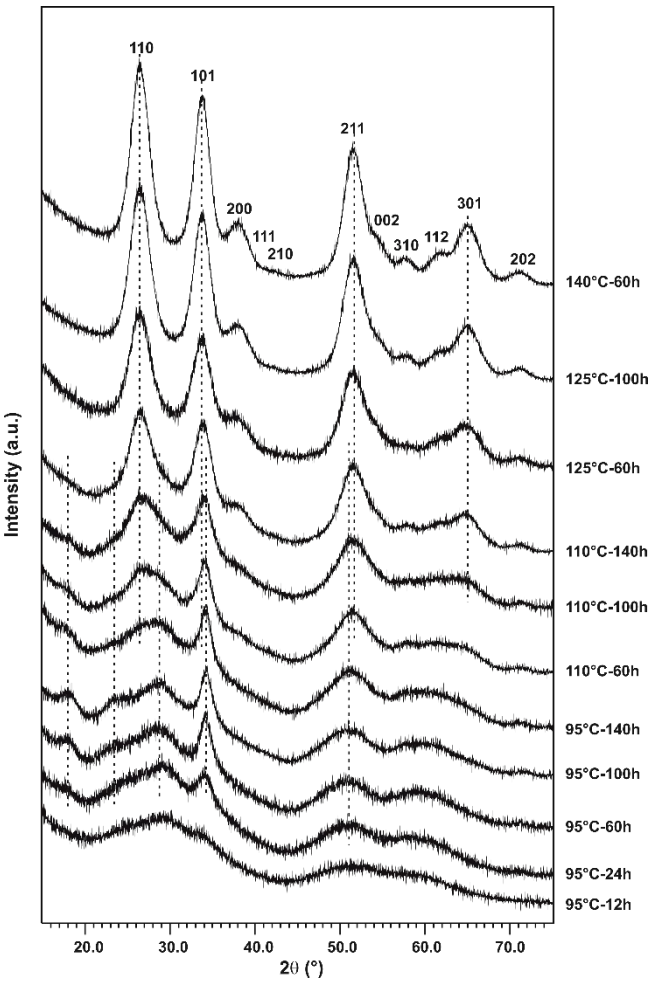

Figure 1. XRD patterns of the samples obtained at different temperatures between 95°C and 140°C for different reaction times in the range of 12 h to 140 h. The pattern of Pr-140°C-60h is indexed according to the rutile-type structure. Dotted lines to guide eye correspond to the main reflections observed on the different patterns.

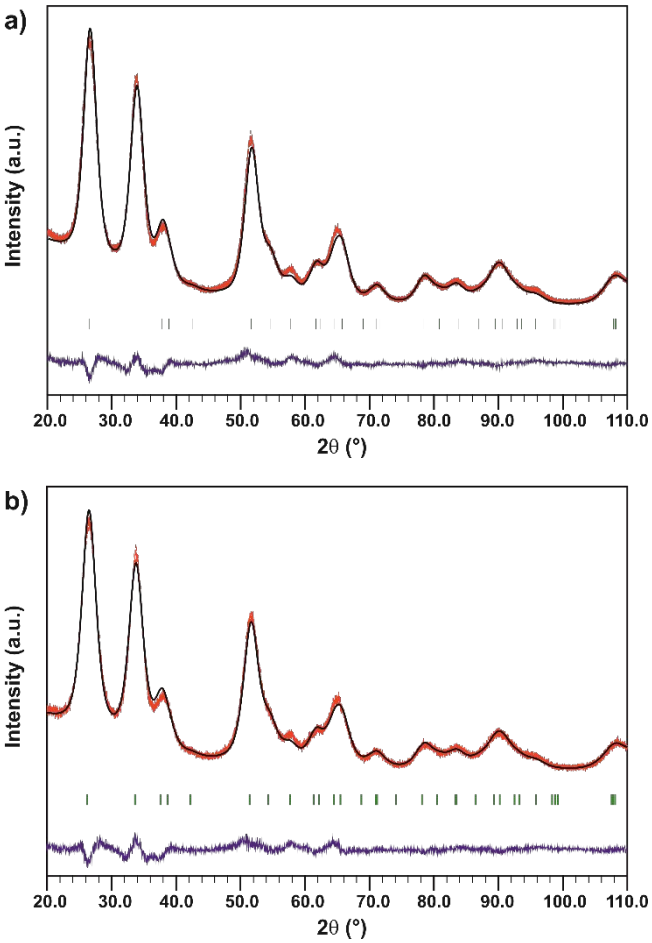

Figure 2. XRD patterns and Rietveld refinements with a rutile-type model for Pr-140°C-60h SnO_2 (a) and Pr-125°C-100h SnO_2 (b) samples.

Despite these strong changes, all XRD patterns share the same global envelop, in particular with common peaks at $2\theta \approx 34°$, 51° and 71° assimilated respectively to the 101, 211 and 202 peaks of the rutile-type structure. These correlations suggest that the structure of the samples undergo a continuous evolution of an intermediate phase toward the rutile-type phase while increasing time and temperature instead of having biphasic samples, as for example a mixture of the rutile-type structure and an unknown metastable phase or a progressive conversion of an amorphous phase into the rutile-type structure.

The evolution of the integral widths of the 211 and 101 peaks as a function of the synthesis conditions is plotted in Figure 3. The first interesting feature is that the 101 line width remains almost constant, whatever the synthesis conditions. From this width, one can estimate using the Scherrer equation a coherent domain size, or correlation length, perpendicular to the (101) planes. We found it is about 2.7 nm. The situation is completely different for the 211 peak, which undergoes large variations with the synthesis conditions. The corresponding correlation lengths vary from a few angstroms (0.7 nm for 95°C-24 h) to a few nanometers (2.8 nm for 140°C-60 h). These observations suggest that a precursor phase of the rutile-type structure is initially formed with a structure relatively well ordered perpendicularly to the (101) lattice planes and almost no order, i.e. a complete loss of coherency, in perpendicular directions. With the increase of the synthesis temperature and reaction time, the structuration of the particles seems to happen gradually along these directions until the final rutile-type is obtained.

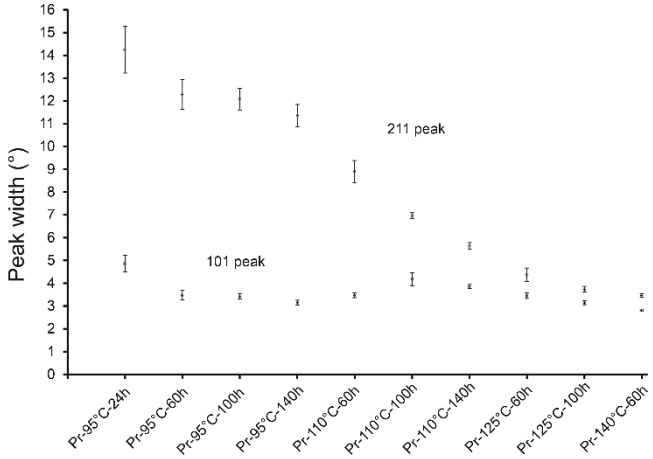

Figure 3. Evolution of the peak width as a function of the synthesis parameters for the samples prepared with $^{i}Pr_2O$.

In order to clarify this possible structuration of the system, TEM measurements were performed on the following selected samples: (i) high temperature synthesis (125°C) for which a pure rutile-

type phase is obtained, (ii) low temperature synthesis (95°C) during the first stages of the structuration when the intermediate phase appears and finally (iii) intermediate temperature synthesis (110°C) during the restructuration of the samples from the intermediate phase to the rutile-type one. All the TEM micrographs are presented in Figure 4.

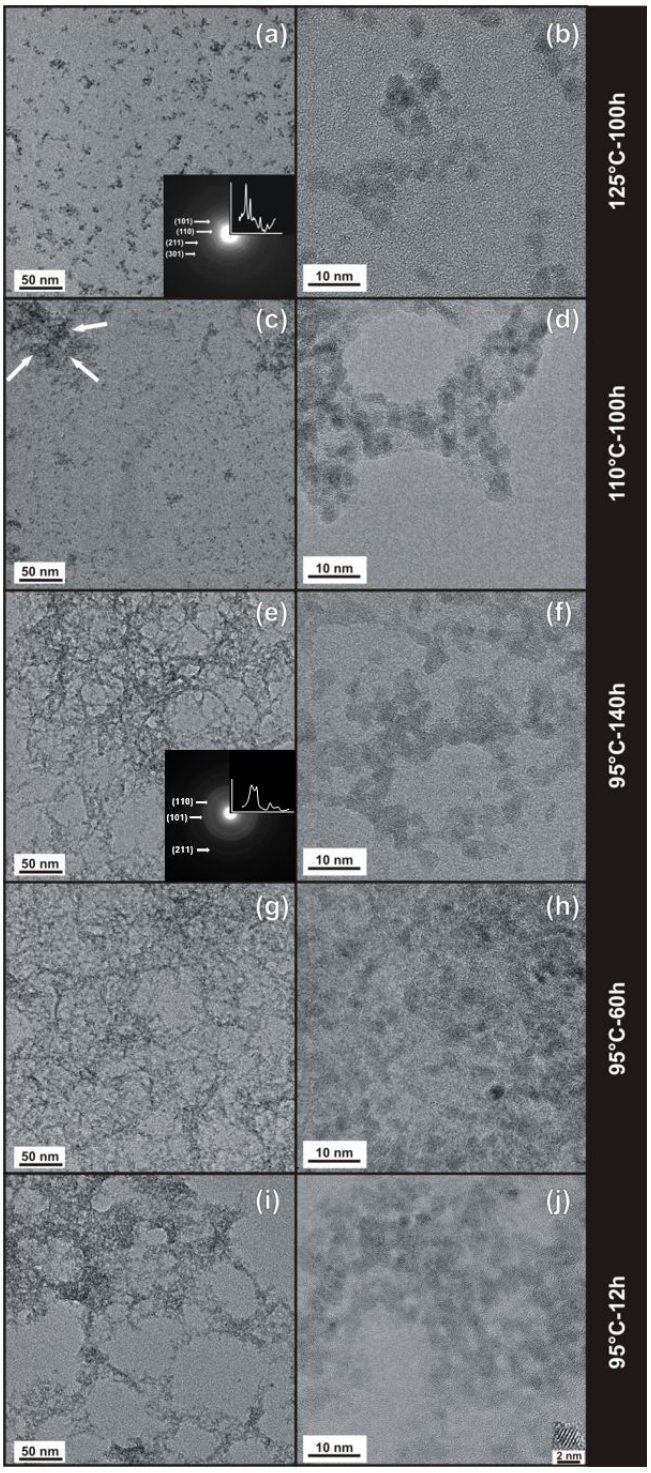

Figure 4. TEM micrographs of Pr-125°C-100h (a and b), Pr-110°C-100h (c and d) Pr-95°C-140h (e and f), Pr-95°C-60h (g and h) and Pr-95°C-12h (i and j). Arrows in (c) indicate heterogeneous

feature. Inset in (a) and (e): SAED pattern and 1D electron powder diffraction diagram obtained with FIT2D.

In the case of the sample synthesized at 125°C for at least 100 h (Figure 4 a-b) isolated and slightly aggregated crystallized nanoparticles are visible. The particles exhibit a spherical or slightly ovoid shape and an estimated size ranging from 2.6 nm up to 4.8 nm with an average size of 3.6 ± 0.3 nm, consistent with the XRD measurements. The SAED pattern shows continuous and broad rings and the corresponding 1D electron powder diffraction diagram is typical of the rutile-type structure. For all the samples obtained at 95°C, a special architectural feature is visible, namely a network of connected crystalline nanoparticles surrounded by an amorphous matrix. The strong chemical contrast between these two phases suggests that the amorphous phase is almost composed of light chemical elements and thus could be organic in nature. For the Pr-95°C-12h sample (Figure 4 i-j), the nanoparticles have a size ranging from 2.2 to 3.2 nm, with an average value of 2.8 ± 0.2 nm. The shape of the nanoparticles is hard to define since they are embedded into the organic phase but it is observed that the nanoparticles are connected to each other without any preferred orientation. For the Pr-95°C-60h sample (Figure 4 g-h), the typical arrangement is still present and no drastic change is observed. For the Pr-95°C-140h sample (Figure 4 e-f), the lace formed by the branching of the organic-nanoparticles mixture looks less dense and seems to tear apart at the periphery of the large assembly shown on the micrographs. At this step, the lace is almost exclusively composed of quasi-spherical nanoparticles stuck together with a very low amount of organics. The Pr-110°C-100h micrographs (Figure 4 c-d) present both characteristics previously exposed, namely isolated nanoparticles or partially agglomerated nanoparticles as well as the specific organic-nanoparticles assembly. Nanoparticles embedded in the organic matrix have

a size of 2.9 ± 0.2 nm while a few isolated nanoparticles, which have certainly underwent a moderate growth, have a size of 3.3 ± 0.2 nm.

On all the TEM micrographs of Figure 4, particles appear crystallized as some lattice planes are clearly resolved. This is also the case for the samples synthesized at low temperature (95°C) for which the XRD patterns have very broad peaks (Figure 1), corresponding to small correlation lengths typical of amorphous phase (Figure 3). This seemingly contradictory observations led us to suspect that the microscope electronic beam could potentially induce crystallization. However, the 1D electron diffraction diagram of Pr-95°C-140h (Figure 4e) is clearly similar to that obtained by XRD (Figure 2), in particular a first broad 110 peak and a second narrow 101 peak. This attests that the electronic beam did not induce crystallization of the samples and that the organic-nanoparticle assembly highlighted by microscopy is indeed representative of the sample, the XRD diagram being more sensitive to the crystalline part of the assembly since the scattering of the organic matrix is low.

By elevating the synthesis temperature and/or extending the reaction time, the disappearance of the organic phase and the formation of rutile-type structure nanocrystals seem to concomitantly happen. Here, we suggest a correlation between the two phenomena. The organic phase could act as a trap for the native nanoparticles and thus limit their growth and restructuration towards the rutile-type structure due to the difficulty for the precursor to diffuse or/and due to a temperature-limited restructuration process.

The reactional mechanism leading to SnO_2 nanocrystals based on the etherolysis of tin chloride thus seems complex. As it is suggested by Aboulaich et al., after an induction period, the tin chloroalkoxide $Sn(O^iPr)_xCl_{4-x}$ issued from the etherolysis of the tin (IV) chloride precursor and/or the native nanoparticles play a catalytic role on the thermal decomposition of ^{i}PrCl, leading to the

formation of propylene and HCl, and then to the polymerization of propylene [15][43][44]. These reactions could be responsible for the formation of the organic or polymeric-nanoparticles assembly that we evidenced for the lower synthesis temperature and shorter reaction time. Upon heating at higher temperature, this original feature progressively disappears and only isolated particles or aggregates are observable. At intermediate temperature (110°C), the double feature of the sample suggests that the polymeric phase is thermally and chemically resorbing since isolated nanoparticles are detected. Polymer degradation is known to be commonly related to thermal and chemical effects [45]. Thereby, the increase of the synthesis temperature and the potential presence of unreacted alkoxide groups trapped inside the polymeric matrix are thought to promote the degradation process and the growth of the nanoparticles. However, since the particles are stuck inside the matrix, due to the lack of mobility of the nanoparticles and to the limited diffusion of reactants, only a slight growth is possible. Once released from the matrix, the particles are free to grow via Ostwald ripening and to restructure into the rutile-type structure. The whole mechanism is non-hydrolytic since no water was evidenced in the synthesis supernatant. As a conclusion, a schematic and simplified summary of this sequence of reactions, leading first to the formation of nanoparticles with the intermediate structure and then to their restructuration into the rutile-type structure, is presented in Figure 5.

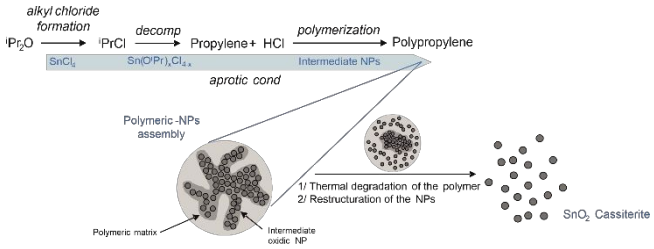

Figure 5. Illustration of the proposed crystallization pathway of SnO_2 nanoparticles synthesized from a mixture of $SnCl_4$ and $^{i}Pr_2O$.

In order to investigate the impact of the solvent on the synthesis route, another ether, i.e. dibenzyl ether, was used. This ether is thought to be susceptible to induce spatial hindrance through its aromatic rings and thus to potentially decrease the particle size. It was also interesting to determine its influence on the crystallization pathway of the nanoparticles. To the best of our knowledge, we describe here the first sol-gel synthesis route of SnO_2 nanocrystals based on the use of dibenzyl ether on tin chloride.

Syntheses with dibenzyl ether. During the washing step, the presence of a colourless liquid phase which was immiscible with the organic solvents used during the procedure was evidenced for all the samples. In contact to this liquid phase, the copper sulphate powder became blue thus highlighting the presence of water in the system. The XRD pattern of the samples synthesized with Bn_2O at 110°C, 125°C and 140°C between 30 min and 60 h are plotted in Figure 6. For 125°C and 140°C they are typical of a single rutile-type phase. The diffraction peaks are broad and the average particle diameters are 2.8 nm and 2.5 nm for the syntheses at 125°C (2 h) and 140°C (0.5 h) respectively. The sample synthesized at 110°C for 60 h has also a diagram typical of the rutile-type phase but with narrower peaks corresponding to an average particle diameter of 3.7 nm. When decreasing the reaction time from 24 h to 4 h, the diagrams evolve similarly to what was observed with $^{i}Pr_2O$, namely they are characteristic of the intermediate phase evidenced previously, with in particular, the presence of very broad peaks at $2\theta = 27°$ and 51° and the narrower peak at 34°. This evolution is however more difficult to evidence because the diagrams are polluted by numerous extra peaks. As the Bn_2O samples exhibit a full organic polymerization of the reaction mixture, these extra peaks are certainly the signature of an organic and/or organometallic crystalline phase impurity. Even if it was not possible to perform TEM observations of the Bn_2O samples because of the large remaining quantity of organic and polymeric phase, we can reasonably assume that the

crystallization process is quite similar for both ethers. Some tests were conducted to limit the production of the polymeric phase by adjusting the reaction time, the temperature, the dilution state but without success. We can also notice that the (Bn_2O-$SnCl_4$) system enables the formation of nanocrystalline material at shorter reaction times than with the ($^iPr_2O$-$SnCl_4$) system.

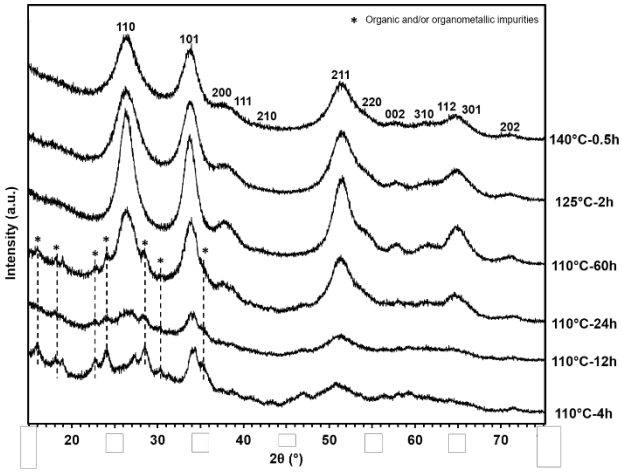

Figure 6. XRD patterns of the samples obtained at different temperatures between 110°C and 140°C for different reaction times in the range of 0.5 h to 60 h. The pattern of Bn-110°C-60h is indexed according to the rutile-type structure.

We now consider the reaction sequence taking place during the nanoparticle synthesis. This is related to the evolution of the initial reaction mixture composed of $SnCl_4$ and Bn_2O at 110°C, which is quite surprising. At the beginning of the reaction, when the temperature is rising to 110°C, the mixture remains brown and translucent. When the temperature reaches 110°C, the mixture becomes opaque, darker, and a boil is noticeable after just a few seconds. Inside the mixture, some colourless translucent drops appear and white solids form at the interface between these drops and the brownish solution. Finally, the precipitate starts to accumulate on the walls of the tube. At the end of the reaction, when the temperature decreases, the mixture is totally opaque, exhibits a caramel-like colour and tends to harden during cooling down. These observations are evidences of three

concomitantly related phenomena during the synthesis: the polymerization of the reactional mixture, the formation of an extra colourless liquid phase and the occurrence of a white precipitate.

Benzyl chloride and dibenzyl ether molecules are well-known to condense and polymerize in certain conditions and in particular when certain Sn-species are present in the chemical system [46][47][48][49]. In particular, in the case of tungsten oxide synthesis from tungsten isopropoxide and benzyl alcohol, Olliges-Stadler *et al.* showed that native tungsten oxide nanowires catalyzed the transformation of benzyl alcohol into dibenzyl ether and then the polymerization reaction of dibenzyl ether into polybenzylene [50]. This reaction sequence led to a dark-blue hard and brittle monolith composed of $W_{18}O_{49}$ nanowires embedded into polybenzylene polymer and also to the release of water in the system. Based on these results, we propose that the polymeric phase we evidenced is formed by the condensation of Bn_2O molecules and/or to the direct polymerization of BnCl issued of the etherolysis of $SnCl_4$ precursor. In both, reaction could be catalyzed by Sn species, and lead to a polymeric matrix related to a member of the polybenzylene family. In addition, as already stated, the colourless liquid phase recovered from the supernatant is water, confirming the release of water during the synthesis. Since we worked with a concentrated mixture of tin chloride and dibenzyl ether, it is not surprising that the polymerization of Bn_2O could be activated and lead to a large release of water. Finally, the third phase, i.e. the white precipitate that appeared at the interface of the aqueous and organic liquid phases, was recovered at the end of the washing step and correspond to the metal oxide nanoparticles.

Considering now the global reaction pathway, we assume that the first step is strictly non-hydrolytic and follows an alkyl halide elimination mechanism. Tin (IV) tetrachloride and/or tin (IV) chloroalkoxide are then susceptible to catalyse dibenzyl ether polymerization and in parallel to form the Sn-O-Sn network via aprotic condensation. The polymerization reaction leads to the

formation of polybenzylene and to the release of water, whose amount is proportional to the initial amount of Bn_2O and the reticulation rate. Water molecules released from dibenzyl ether condensation are then susceptible to switch the non-hydrolytic sol-gel process to a hydrolytic one. Doing so, they promote the precursor condensation, the particle nucleation and possibly the particle restructuration from the intermediate phase toward the final rutile-type structure, in particular in shorter time than with $^{i}Pr_2O$ at 110°C.

As a conclusion, a simplified scheme of these successive steps, involved in the formation of the SnO_2 nanoparticles *via* the etherolysis of $SnCl_4$ by Bn_2O, is presented Figure 7.

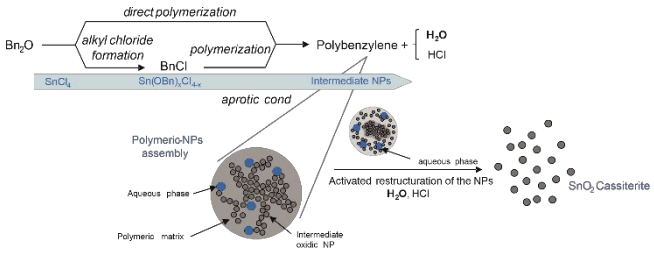

Figure 7. Illustration of the proposed crystallization pathway of SnO_2 nanoparticles synthesized from a mixture of $SnCl_4$ and Bn_2O.

Comparison of the two systems. In both systems, the reaction of ethers on tin (IV) tetrachloride lead to an original nanoparticle crystallization pathway involving the early formation of an intermediate precursor phase which progressively converts into the rutile-type structure. This is accompanied by the production of a polymer phase in variable quantity. We assume that the etherolysis/condensation reactions, leading to the intermediate phase formation, and the condensation/polymerization reactions, leading to the polymer formation, happen simultaneously. The polymeric phase then acts as a trap for the primary nanocrystals until the restructuration is possible.

In the case of diisopropyl ether, the polymerization is limited and confined near the particle surface leading to the formation of the nanoparticle-polymer assembly observable on the TEM micrographs (Figure 4). The restructuration depends then of the polymer degradation which releases the particles. In the case of the use of dibenzyl ether, the formation of the polymeric phase is more significant and the restructuration mechanism seems to happen essentially through the release of water in the system. The compounds presenting aromatic rings, typically benzyl alcohol, dibenzyl ether and benzyl chloride, show a great ability to polymerize, particularly in the presence of tin (IV) tetrachloride, [47] and by this way are susceptible to produce hydrochloric acid and/or water (for benzyl alcohol and dibenzyl ether). This ability seems to be less exacerbated in the case of ethers which do not have aromatic ring, such as diisopropyl ether [44]. The difference of reactivity between the two systems is probably related to the solvents properties and in particular to their capacity to polymerize and to produce water since water promotes hydrolytic sol-gel reactions and the restructuration of the intermediate nanoparticles into rutile-type ones at much shorter reaction times.

For both ethers, nanoparticles with the expected rutile-type structure were obtained with similar sizes of about 3 nm. Rather than the ability of the solvent to induce spatial hindrance, as we initially supposed for dibenzyl ether, it is more the way it affects the crystallization pathway by polymerizing, which controls the nanoparticle structure and size. Indeed, since the formation of the intermediate oxide phase and its restructuration cannot be circumvented, such steps need to be understood and be taken into account in order to produce small-size-controlled tin oxide nanocrystals with the rutile-type structure. That is why the good knowledge of the properties and the reactivity of all the reactants involved in the synthesis is necessary.

Conclusion

In this study, the early stages of the synthesis of small tin oxide nanocrystals *via* the etherolysis of tin (IV) tetrachloride was investigated with diisopropyl or dibenzyl ether as oxygen donors. The results obtained from the study of the structural and morphological features obtained by XRD and TEM indicate a more complex crystallization pathway than previously reported in the literature. The SnO_2 nanocrystals synthesis begins, first, by the formation of a nanocrystalline inorganic intermediate phase embedded in a polymeric phase forming a large complex assembly. The structure of the intermediate phase is partially ordered and exhibits strong similarities with the rutile-type structure. In the case of diisopropyl ether, the degradation of the polymer matrix allows the nanoparticle restructuration into the rutile-type structure when the synthesis temperature and reaction time are sufficient. In the case of dibenzyl ether, the full polymerization of the reactional mixture is accompanied by the formation of water. The polymer, which is supposed to be a member of the polybenzylene family, is produced by the condensation of dibenzyl ether and/or benzyl chloride both catalysed by tin (IV) tetrachloride. The water release by the condensation of ether molecules seems to promote and activate the restructuration of the nanoparticles. In both cases, the occurrence of the intermediate phase cannot be circumvented and SnO_2 nanoparticles of 2-4 nm with rutile-type structure are finally obtained.

The formation of rutile-type SnO_2 nanoparticles of very small size goes through a fine control of the crystallization pathway. The formation of the polymeric phase shows that the properties of both ether-$SnCl_4$ couples and the formed nanocrystals has to be taken into account to control the final product. Moreover, the formation of water in a non-hydrolytic synthesis route indicates that the byproducts could also play a crucial role in the formation of the final oxide nanocrystals.

Author information

Corresponding author

*Email: olivier.masson@unilim.fr

ORCID: 0000-0003-0036-3859

Author contributions

All authors have given approval to the final version of the manuscript.

Notes

The authors declare no competing financial interest.

Acknowledgments

We acknowledge Pierre Carles for the TEM measurements and for the support in the analysis of the micrographs.

References

[1] M. Batzill and U. Diebold, « The surface and materials science of tin oxide », *Prog. Surf. Sci.*, vol. 79, nº 2, p. 47-154, 2005.

[2] Z. Zhang, X. Zou, L. Xu, L. Liao, W. Liu, J. Ho, X. Xiao, C. Jiang and J. Lia, « Hydrogen gas sensor based on metal oxide nanoparticles decorated graphene transistor », *Nanoscale*, vol. 7, nº 22, p. 10078-10084, 2015.

[3] S. Das and V. Jayaraman, « SnO_2: A comprehensive review on structures and gas sensors », *Prog. Mater. Sci.*, vol. 66, p. 112-255, 2014.

[4] S. Wang, J. Huang, Y. Zhao, S. Wang, X. Wang, T. Zhang, S. Wu, S. Zhang and W. Huang, « Preparation, characterization and catalytic behavior of SnO_2 supported Au catalysts for low-temperature CO oxidation », *J. Mol. Catal. Chem.*, vol. 259, nº 1-2, p. 245-252, 2006.

[5] P. Rajaram, Y. C. Goswami, S. Rajagopalan and V. K. Gupta, « Optical and structural properties of SnO_2 films grown by a low-cost CVD technique », *Mater. Lett.*, vol. 54, nº 2-3, p. 158-163, 2002.

[6] T. Sahm, L. Mädler, A. Gurlo, N. Barsan, S. E. Pratsinis and U. Weimar, « Flame spray synthesis of tin dioxide nanoparticles for gas sensing », *Sens. Actuators B Chem.*, vol. 98, nº 2-3, p. 148-153, 2004.

[7] S. M. Ingole, S. T. Navale, Y. H. Navale, D. K. Bandgar, F. J. Stadler, R. S. Mane, N. S. Ramgir, S. K. Gupta, D. K. Aswal and V. B. Patil, « Nanostructured tin oxide films: Physical synthesis, characterization, and gas sensing properties », *J. Colloid Interface Sci.*, vol. 493, p. 162-170, 2017.

[8] M. K. Patel, J. Singh, M. K. Singh, V. V. Agrawal, S. G. Ansari and B. D. Malhotra, « Tin oxide quantum dot based DNA sensor for pathogen detection », *J. Nanosci. Nanotechnol.*, vol. 13, nº 3, p. 1671-1678, 2013.

[9] E. R. Leite, E. J. H. Lee, T. R. Giraldi, F. M. Pontes and E. Longo, « A simple and novel method to synthesize doped and undoped SnO_2 nanocrystals at room temperature », *J. Nanosci. Nanotechnol.*, vol. 4, nº 7, p. 774-778, 2004.

[10] N. M. Shaalan, D. Hamad, A. Y. Abdel-Latief and M. A. Abdel-Rahim, « Preparation of quantum size of tin oxide: Structural and physical characterization », *Prog. Nat. Sci. Mater. Int.*, vol. 26, n° 2, p. 145-151, 2016.

[11] M. Epifani, E. Pellicer, J. Arbiol and J. R. Morante, « Metal oxide nanocrystals from the injection of metal oxide sols in a coordinating environment: Principles, applicability, and investigation of the synthesis variables in the case study of CeO_2 and SnO_2 », *Chem. Mater.*, vol. 21, n° 5, p. 862-870, 2009.

[12] J. S. Chen and X. W. Lou, « SnO_2-based nanomaterials: Synthesis and application in lithium-ion batteries », *Small*, vol. 9, n° 11, p. 1877-1893, 2013.

[13] H. Zhu, D. Yang, G. Yu, H. Zhang and K. Yao, « A simple hydrothermal route for synthesizing SnO_2 quantum dots », *Nanotechnology*, vol. 17, n° 9, p. 2386-2389, 2006.

[14] S. Gnanam and V. Rajendran, « Influence of ethylene glycol on the nanostructured pure and V-doped SnO_2 nanoparticles via sol-gel process and application in photocatalysts », *J. Optoelectron. Adv. Mater.*, vol. 12, n° 11, p. 2199-2207, 2010.

[15] A. Aboulaich, B. Boury and P. H. Mutin, « Reactive and organosoluble SnO_2 nanoparticles by a surfactant-free non-hydrolytic sol-gel route », *Eur. J. Inorg. Chem.*, n° 24, p. 3644-3649, 2011.

[16] J. Ba, J. Polleux, M. Antonietti and M. Niederberger, « Non-aqueous synthesis of tin oxide nanocrystals and their assembly into ordered porous mesostructures », *Adv. Mater.*, vol. 17, n° 20, p. 2509-2512, 2005.

[17] N. Pinna, G. Neri, M. Antonietti and M. Niederberger, « Nonaqueous synthesis of nanocrystalline semiconducting metal oxides for gas sensing », *Angew. Chem. - Int. Ed.*, vol. 43, nº 33, p. 4345-4349, 2004.

[18] M. Niederberger and N. Pinna, « Metal Oxide Nanoparticles in Organic Solvents: Synthesis, Formation, Assembly and Application », *London: Springer-Verlag*, 2009.

[19] P. H. Mutin and A. Vioux, « Nonhydrolytic Processing of Oxide-Based Materials: Simple Routes to Control Homogeneity, Morphology, and Nanostructure », *Chem. Mater.*, vol. 21, nº 4, p. 582-596, 2009.

[20] A. Vioux, « Nonhydrolytic Sol−Gel Routes to Oxides », *Chem. Mater.*, vol. 9, nº 11, p. 2292-2299, 1997.

[21] M. Niederberger and H. Cölfen, « Oriented attachment and mesocrystals: Non-classical crystallization mechanisms based on nanoparticle assembly », *Phys. Chem. Chem. Phys.*, vol. 8, nº 28, p. 3271-3287, 2006.

[22] J. F. Banfield, S. A. Welch, H. Zhang, T. T. Ebert and R. L. Penn, « Aggregation-based crystal growth and microstructure development in natural iron oxyhydroxide biomineralization products », *Science*, vol. 289, nº 5480, p. 751-754, 2000.

[23] S. Sun, D. Gebauer and H. Cölfen, « Alignment of Amorphous Iron Oxide Clusters: A Non-Classical Mechanism for Magnetite Formation », *Angew. Chem. - Int. Ed.*, vol. 56, nº 14, p. 4042-4046, 2017.

[24] B. Ludi and M. Niederberger, « Zinc oxide nanoparticles: Chemical mechanisms and classical and non-classical crystallization », *Dalton Trans.*, vol. 42, nº 35, p. 12554-12568, 2013.

[25] D. Gebauer, A. Völkel and H. Cölfen, « Stable prenucleation calcium carbonate clusters », *Science*, vol. 322, nº 5909, p. 1819-1822, 2008.

[26] Z. Zhuang, J. Zhang, F. Huang, Y. Wang and Z. Lin, « Pure multistep oriented attachment growth kinetics of surfactant-free SnO_2 nanocrystals », *Phys. Chem. Chem. Phys.*, vol. 11, nº 38, p. 8516-8521, 2009.

[27] D. G. Stroppa, L. A. Montoro, A. Beltrán, T. G. Conti, R. O. da Silva, J. Andres, E. R. Leite and A. J. Ramirez, « Anomalous oriented attachment growth behavior on SnO_2 nanocrystals », *Chem. Commun.*, vol. 47, nº 11, p. 3117-3119, 2011.

[28] R. L. Penn and J. F. Banfield, « Imperfect oriented attachment: Dislocation generation in defect-free nanocrystals », *Science*, vol. 281, nº 5379, p. 969-971, 1998.

[29] E. J. H. Lee, C. Ribeiro, E. Longo and E. R. Leite, « Oriented attachment: An effective mechanism in the formation of anisotropic nanocrystals », *J. Phys. Chem. B*, vol. 109, nº 44, p. 20842-20846, 2005.

[30] D. Zitoun, N. Pinna, N. Frolet and C. Belin, « Single crystal manganese oxide multipods by oriented attachment », *J. Am. Chem. Soc.*, vol. 127, nº 43, p. 15034-15035, 2005.

[31] H. Cölfen and M. Antonietti, « Mesocrystals: Inorganic superstructures made by highly parallel crystallization and controlled alignment », *Angew. Chem. - Int. Ed.*, vol. 44, nº 35, p. 5576-5591, 2005.

[32] R.-Q. Song and H. Cölfen, « Mesocrystals - Ordered nanoparticle superstructures », *Adv. Mater.*, vol. 22, nº 12, p. 1301-1330, 2010.

[33] J. Ba, A. Feldhoff, D. F. Rohlfing, M. Wark, M. Antonietti and M. Niederberger, « Crystallization of indium tin oxide nanoparticles: From cooperative behavior to individuality », *Small*, vol. 3, nº 2, p. 310-317, 2007.

[34] H. M. Rietveld, « A profile refinement method for nuclear and magnetic structures », *J. Appl. Crystallogr.*, vol. 2, nº 2, p. 65-71, 1969.

[35] R. A. Young, « The Rietveld Method », Oxford University Press, 1995.

[36] J. Rodríguez-Carvajal, « Recent advances in magnetic structure determination by neutron powder diffraction », *Phys. B Condens. Matter*, vol. 192, nº 1, p. 55-69, oct. 1993.

[37] T. Roisnel and J. Rodríguez-Carvajal, « WinPLOTR: A windows tool for powder diffraction pattern analysis », *Mater. Sci. Forum*, vol. 378-381, nº I, p. 118-123, 2001.

[38] O. Masson, « Peakoc ». http://www.esrf.eu/computing/scientific/PEAKOC/MAIN.htm.

[39] P. Thompson, D. E. Cox and J. B. Hastings, « Rietveld refinement of Debye–Scherrer synchrotron X-ray data from Al_2O_3 », *J. Appl. Crystallogr.*, vol. 20, nº 2, p. 79-83, 1987.

[40] J. I. Langford, « A rapid method for analysing the breadths of diffraction and spectral lines using the Voigt function », *J. Appl. Crystallogr.*, vol. 11, nº 1, p. 10-14, 1978.

[41] P. Scherrer, « Bestimmung der Größe und der inneren Struktur von Kolloidteilchen mittels Röntgenstrahlen », *Nachrichten Von Ges. Wiss. Zu Gött. Math.-Phys. Kl.*, vol. 1918, p. 98-100, 1918.

[42] A. P. Hammersley, « FIT2D: a multi-purpose data reduction, analysis and visualization program », *J. Appl. Crystallogr.*, vol. 49, nº 2, p. 646-652, 2016.

[43] T. Matsumoto, T. Nakano, Y. Yokoyama and T. Makiguchi, « Process for producing isopropyl chloride », US20040215041A1, 2004.

[44] F. H. Gayer, « The Catalytic Polymerization of Propylene », *Ind. Eng. Chem.*, vol. 25, nº 10, p. 1122-1127, 1933.

[45] L. Shibryaeva, « Thermal Oxidation of Polypropylene and Modified Polypropylene - Structure Effects ». INTECH Open Access Publisher, 2012.

[46] C. P. Tsonis, « Homogeneous catalytic polymerization of benzyl chloride leading to linear high molecular weight polymers: an elusive goal », *J. Mol. Catal.*, vol. 57, nº 3, p. 313-323, 1990.

[47] T. M'Hiri, C. Catusse, R. Catusse and J. L. J. Dubry, « Polymerization of benzyl alcohol and its derived compounds with an ion exchange resin », *React. Kinet. Catal. Lett.*, vol. 22, nº 3-4, p. 425-428, 1983.

[48] R. A. Jacobson, « Polymers from benzyl chloride and related compounds », *J. Am. Chem. Soc.*, vol. 54, nº 4, p. 1513-1518, 1932.

[49] O. C. Dermer and E. Hooper, « Catalysts for the Polymerization of Benzyl Chloride », *J. Am. Chem. Soc.*, vol. 63, nº 12, p. 3525-3526, 1941.

[50] I. Olliges-Stadler, M. D. Rossell and M. Niederberger, « Co-operative formation of monolithic tungsten oxide-polybenzylene hybrids via polymerization of benzyl alcohol and study of the catalytic activity of the tungsten oxide nanoparticles », *Small Weinh. Bergstr. Ger.*, vol. 6, nº 8, p. 960-966, 2010.

TOC graphic and synopsis

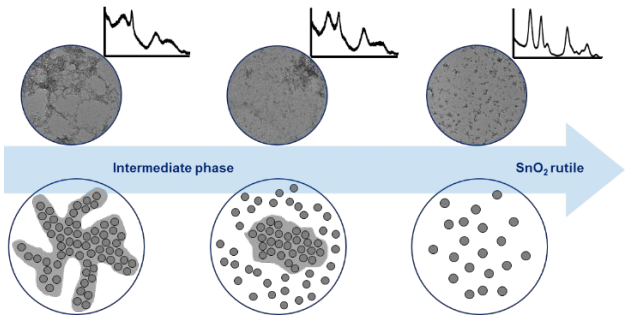

For table of content only

Synopsis. The crystallization pathways of tin dioxide nanoparticles synthesized by a nonaqueous sol-gel method based on the etherolysis of a tin (IV) tetrachloride precursor was investigated. Two ethers were used as oxygen donor, namely diisopropyl ether and dibenzyl ether. In both cases, the formation of ultra-small nanoparticles proceed via an original and complex pathway involving the progressive transformation of an intermediate phase as well as the formation of a polymeric phase.